Spectrochimica Acta Part B 173 (2020) 105987

Contents lists available at ScienceDirect

Spectrochimica Acta Part B

journal homepage: www.elsevier.com/locate/sab

Species distribution in laser-induced plasma on the surface of binary miscible alloy

Yang Zhao[a], Lei Zhang[a,b,*], Shuqing Wang[c], Jianghua Han[c], Guofu Xia[c], Weiguang Ma[a,b], Lei Dong[a,b], Wangbao Yin[a,b,*], Liantuan Xiao[a,b], Suotang Jia[a,b], Jin Yu[d]

[a] State Key Laboratory of Quantum Optics and Quantum Optics Devices, Institute of Laser Spectroscopy, Shanxi University, Taiyuan 030006, China
[b] Collaborative Innovation Center of Extreme Optics, Shanxi University, Taiyuan 030006, China
[c] National Energy R&D Center of Petroleum Refining Technology, RIPP, SINOPEC, China
[d] School of Physics and Astronomy, Shanghai Jiao Tong University, Shanghai 200240, China

ARTICLE INFO

Keywords:
Species distribution
Laser-induced plasma (LIP)
Laser-induced breakdown spectroscopy (LIBS)
Laser-supported absorption (LSA) wave

ABSTRACT

The spatiotemporal species distribution and dynamics of plasma play a crucially important role in improving the quality of the deposited film fabricated by pulsed laser deposition (PLD) and optimizing the spectral acquisition to enhance the quantitative performance of spatial-resolved laser-induced breakdown spectroscopy (LIBS). In this work, the monochrome imaging is used to analyze the plasmas induced from binary miscible alloys and explore the dependence of species distribution in plasma on laser-supported combustion (LSC) and laser-supported detonation (LSD) wave propagation regimes. This paper includes three conclusions: 1) the species distribution in LSC-wave dominated plasma induced from immiscible alloy is heavily influenced by the melting points of constituted elements, while in LSC-wave dominated plasma induced from miscible alloy, it is related to the boiling points; 2) whether the alloy is miscible or immiscible, the species distribution in LSD-wave dominated plasma is only related to the atomic masses; 3) to a great extent, the reduction rate of species in LSC-wave dominated plasma is associated with the transition probability, while that in LSD-wave dominated plasma is associated with the number density of species in the upper energy level.

1. Introduction

Laser-induced plasma (LIP) concerns many technological applications, such as the material production by pulsed laser deposition (PLD) [1,2] and the rapid industrial analysis by laser-induced breakdown spectroscopy (LIBS) [3–5]. The processes of LIP generation and propagation are very complicated, which mainly involve the knowledge of fluid-dynamics, radiation transport, equilibrium deviation, chemical reactivity and ablation mechanisms, and even some unsolved problems [6]. When the laser irradiance is high enough and exceeds the ablation threshold, the target will interact strongly with the laser. Under the heating of the leading edge of laser pulse, the temperature of the ablation zone on the target surface increases sharply, and the target material is instantly melted and vaporized. The vapor is ejected from the target surface at supersonic speed, so that the ambient gas at the contact surface is compressed to form a shocked gas layer. The absorption of subsequent laser by vapor and shocked gas are responsible for the formation of laser-supported absorption (LSA) wave, which corresponds to the plasma shielding effect and affects the subsequent evolution of plasma. According to whether the laser energy is mainly absorbed by vapor or shocked gas, two major LSA-waves are known as: laser-supported combustion (LSC) wave and laser-supported detonation (LSD) wave. For LSC-wave, the plasma shielding occurs in the ablation vapor located in the middle of the plasma, while for LSD-wave, it occurs in the shocked ambient gas located in the propagation front of the plasma [7–11].

Investigation on the spatiotemporal distribution and evolution of species in the process of plasma expansion can deepen our understanding of plasma generation and propagation, and may further optimize the application of LIP related technologies. For example, the quality of film deposited by PLD is highly dependent on the density of species distribution in LIP [12], while the intensity of spectral lines in spatially resolved LIBS emission spectra depends on the spatiotemporal distribution of atoms, ions, electrons and temperature in the plasma. In recent years, many research papers on spatially resolved plasma emission have been published [13–22], but few have studied the

* Corresponding authors at: State Key Laboratory of Quantum Optics and Quantum Optics Devices, Institute of Laser Spectroscopy, Shanxi University, Taiyuan 030006, China.
E-mail addresses: k1226@sxu.edu.cn (L. Zhang), ywb65@sxu.edu.cn (W. Yin).

https://doi.org/10.1016/j.sab.2020.105987
Received 29 July 2020; Received in revised form 21 September 2020; Accepted 22 September 2020
Available online 24 September 2020
0584-8547/

relationship between propagation regime and species distribution of plasma.

As the most common sample in LIBS analysis, the alloy has relatively simple structure and homogeneous distribution, which is very suitable for the study of plasma propagation and species distribution. According to the characteristics of liquid phase separation, alloys can be divided into immiscible and miscible alloys. In our previous work [23], we investigated the species distribution in the plasma generated from immiscible Al-Sn alloy and explored the dependence of species distribution in plasma on LSA-wave regime. It has been proved that when the surface temperature of the immiscible alloy is higher than the melting point of one of the constituted elements, the pure liquid of this element will be separated from the solid mixture during laser ablation and distributed in the upper shell of the plasma. However, the physical properties of miscible alloys are quite different from those of immiscible alloys, and they do not have the characteristics of liquid phase separation. Therefore, when the surface temperature reaches the melting point of the alloy, all the constituted elements will be melted at the same time. Therefore, an extended discussion is necessary to study the spatiotemporal distribution structure of plasma induced from miscible alloy and analyze the dependence of species distribution in plasma on LSA-wave regime.

In this paper, the dual-wavelength differential spectroscopic imaging is used to obtain the spatiotemporal distribution of species in LSC- and LSD-wave dominated plasmas induced from binary miscible alloys. The dependence of species distribution on LSA-wave regime and the lifetimes of species in LSC- and LSD-wave dominated plasmas are also studied.

2. Experimental

2.1. Sample

Al-Mg alloy as a miscible alloy has obvious liquid phase separation characteristics. It can be seen from Table 1 that the melting points of aluminum and magnesium are similar, but the boiling points are quite different. Therefore, the species distribution determined by melting or boiling point is easy to distinguish. Moreover, the characteristic emission lines of aluminum and magnesium are sparse and non-interferential, so Al-Mg alloy is very suitable for experimental research. The mass ratio of Al to Mg in the alloy used in this experiment is 49:1, which corresponds to an atomic number density ratio of about 44:1.

2.2. Experimental setup

The experimental LIBS system with differential spectroscopic imaging has been described in detail in our previous work [23]. The laser emitted by a Nd: YAG laser (Spectra Physics, INDIHG-20S, wavelength: 1064 nm, repetition rate: 20 Hz) was focused by a lens with 50 mm focal length and used for ablation in two LSA-wave regimes. The irradiance corresponding to pulse energy of 6 mJ was1.2 GW/cm^2 (close to the breakdown threshold of Al-Mg alloy), and that of 50 mJ was 10 GW/cm^2. The argon was continuously blown at a flow rate of 5 L/min by a pair of tubes mounted on both sides of the plasma to ensure the background gas was always argon.

In the spectrum measurement part, the plasma image was magnified 6 times by lens along the axis perpendicular to the propagation axis of laser beam. An all-silica optical fiber with diameter of 0.2 mm was installed on an X-Y stage and moved along the plasma image to collect the emission came from different axial (x) and radial (r) positions of the plasma. And then the spatial resolved optical signal was sent to a grating spectrograph (Princeton Instruments, SP-2750) equipped with an ICCD (Princeton Instruments, PI-MAX4-1024i).

In the dual-wavelength differential spectroscopic imaging part, the plasma was imaged on the ICCD (Andor, iStar DH334T) by a 4f system consisting of two lens. The delay times was set to 100, 150, 200, 400 and 800 ns, and the corresponding gate widths were 5, 5, 5, 20 and 30 ns, respectively. The images of species in plasma were filtered by a pair of narrow band filters (F1 and F2), in which F1 was centered on the characteristic line of the species of interest, and the central wavelength of F2 was shifted nearby this line. Therefore, by subtracting the contribution of the continuous background recorded by F2 from the species images recorded by F1, the two-dimensional emission of species in plasma was obtained. But these images were the integral intensity along the line of sight. To obtain spatial resolved images, the Abel inversion [24] based on Fourier-Hankel algorithm was carried out. In order to get images with good signal-to-noise ratio and low-fluctuation, more than 60 plasmas were accumulated in each image with an appropriate ICCD gain (Table 1). Because each species has its own emission intensity and ICCD gain coefficient, the brightness difference between emissivity images will be so large that it is difficult to compare them in one image without normalization. Therefore, the emissivity images were normalized by their maximums and the Red-Green-Blue (RGB) color model was applied to multi-species plasma image display by using the image processing program. Specifically, the monochromatic images of each species were superimposed in Photoshop in “screen” layer blending mode.

Fig. 1 shows the spectra of plasma induced from Al-Mg alloy by laser irradiance of 10 GW/cm^2 at 100 ns and 400 ns. The selected emission lines on behalf of the species of Al, Mg, and Ar are indicated by letters “a, c, d, f, e and h” for Al II, Al I, Mg II, Mg I, Ar II and Ar I, respectively. And the letters “b”, “g” and “i” represent the continuum emissions. The

Table 1
Specifications of the physical properties of Al and Mg, the wavelengths, lower and upper level energies and transition probabilities of emission lines selected, the central wavelengths of filters used to observe species and the ICCD gains for the given species under different laser irradiances.

Element	Melting point (K)	Boiling point (K)	Relative atomic mass	Species	Emission line (nm)	Lower level energy (eV)	Upper level energy (eV)	Transition probability ($\times 10^7$ s^{-1})	Central wavelength of F1 (nm)	Central wavelength of F2 (nm)	ICCD gain	
											1.2 GW/cm^2	10 GW/cm^2
Aluminum	933	2740	27	Al I	394.40	0.00	3.14	4.99	396	365	600	0
					396.15	0.01	3.14	9.85				
				Al II	358.66	11.85	15.30	23.5	358	365	600	0
Magnesium	923	1363	24	Mg I	516.73	2.71	4.33	2.80	520	530	1000	0
					517.27	2.71	5.11	1.13				
					518.36	2.72	5.11	3.37				
				Mg II	448.11	8.86	11.63	23.3	530	522	1000	0
					448.13	8.86	11.63	21.7				
Argon	–	–	–	Ar I	763.51	11.55	13.17	2.45	764	786	1000	0
				Ar II	484.78	16.75	19.31	8.49	488	530	1000	0
					487.99	17.14	19.68	8.23				

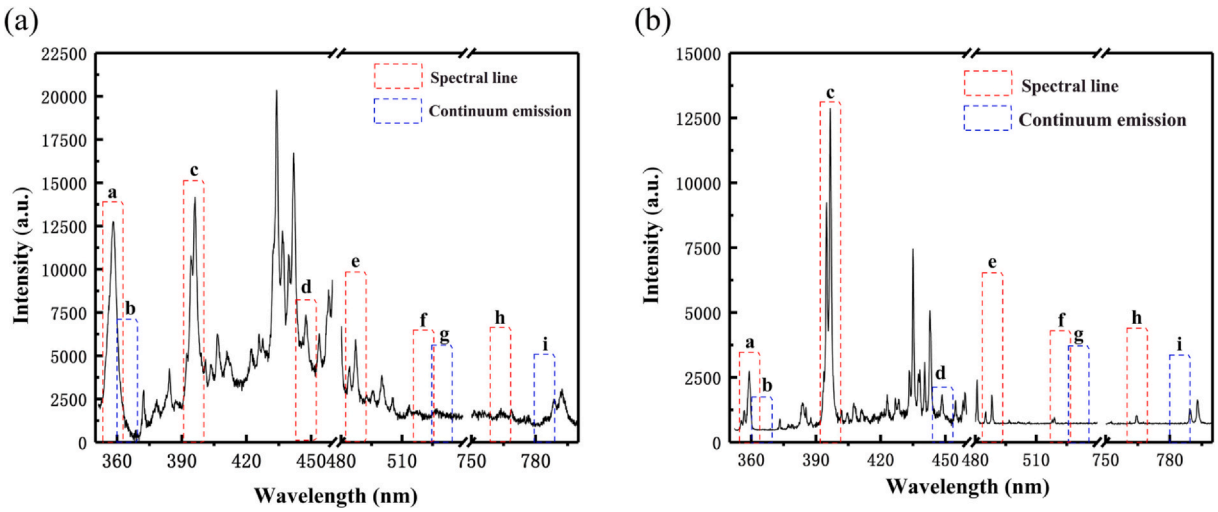

Fig. 1. Spectra of the central part of plasma induced from Al-Mg alloy by laser irradiance of 10 GW/cm^2 at (a) 100 ns and (b) 400 ns. The letters from "a" to "i" represent the emission lines used for spectral imaging of Al II (a), Al I (c), Mg II (d), Mg I (f), Ar II (e) and Ar I (h), and the letters "b", "g", and "i" represent the continuum emission.

wavelengths, lower and upper level energies and transition probabilities of emission lines selected to represent various species, and the central wavelengths of filters used to get species images are also listed in Table 1.

It should be known that the spatial distribution of line intensity can represent the spatial number density distribution of corresponding element after correcting the electron temperature and electron number density of plasma. Whereas, the purpose of this work is to qualitatively analyze the plasma morphology and structure, rather than to quantitatively analyze the spatial distribution of species density. Therefore, it is not necessary to correct the intensity of spectral lines in this work.

3. Results and discussion

In order to study the morphology, species distribution and internal structure of plasmas produced from miscible binary alloy in different propagation regimes, the evolution of the emissivity images of species in plasmas were observed under low and high laser irradiances, respectively, and the results are shown in Fig. 2. Various colors were used to represent different species: Ar I (blue), Ar II (grey), Al I (red), Al II (green), Mg I (goldenrod) and Mg II (fuchsia). The results were discussed as follows.

3.1. Identification of LSA-wave regime

The internal structure of plasma and the species distribution of Al, Mg and Ar are shown in Fig. 2, but it is difficult to distinguish due to partially overlapped colors. For clear vision, the results of Fig. 2 are shown separately in Fig. 3 for Al and Ar and Fig. 4 for Mg and Ar. The normalized central axial emissivity profiles of Ar I, Ar II, Al I, Al II, Mg I, and Mg II species in plasmas produced by laser irradiances of 1.2 GW/cm^2 and 10 GW/ cm^2 at 100 ns are shown in Fig. 5. It can be seen that at the same time, the size of plasma induced by laser irradiance of 10 GW/cm^2 is larger than that induced by laser irradiance of 1.2 GW/cm^2. This is because the higher the induced laser energy, the greater the axial and radial velocities of plasma. The common feature of the two species distribution is that the Ar species were located at the outer layer of plasma, while the Mg and Al species from the target were located at the inner layer.

When the plasma was induced by high laser irradiance (10 GW/cm^2), the argon at the top of the plasma was completely ionized at the early stage (100–150 ns), the argon atoms were only distributed at the lower part of the outer layer of plasma, and the argon ions disappeared at 800 ns. The high ionization degree and the slow decay of the ionized population of shocked background argon indicated that the shocked gas absorbed a large quantity of laser radiaton without requiring any additional energy from the hot plasma core. According to the such high ionizability of argon, it can be concluded that LSD-wave was the main

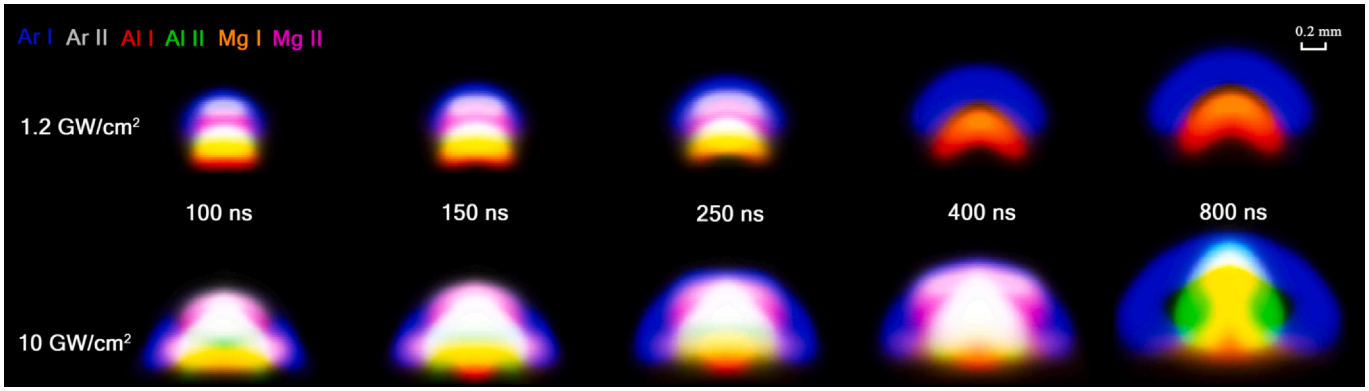

Fig. 2. Emissivity images of Ar I, Ar II, Al I, Al II, Mg I, and Mg II species in the plasmas produced from Al-Mg alloy at 100, 150, 200, 400, and 800 ns by laser irradiances of 1.2 GW/cm^2 and 10 GW/cm^2.

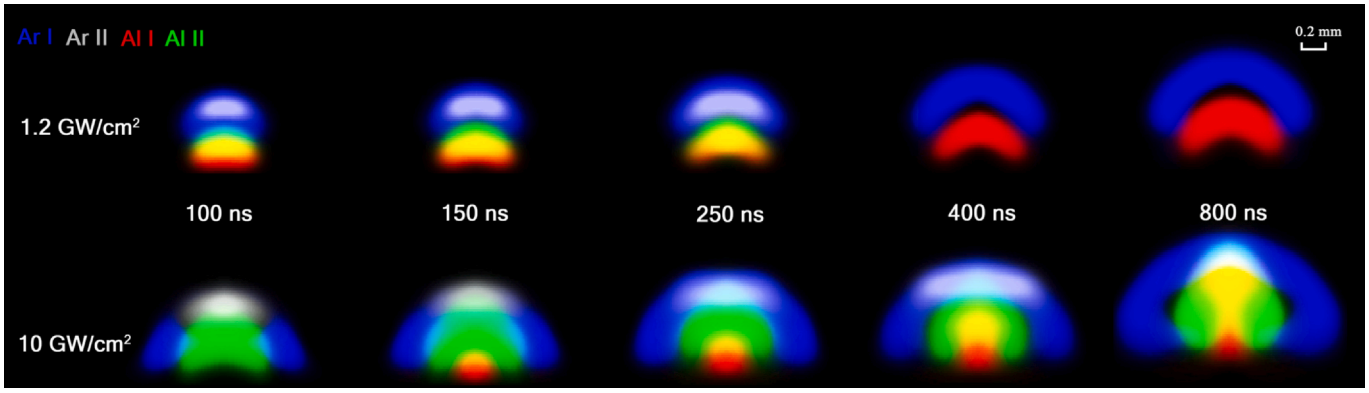

Fig. 3. Emissivity images of Ar I, Ar II, Al I, and Al II species in plasmas produced from the Al-Mg alloy at 100, 150, 200, 400, and 800 ns by laser irradiances of 1.2 GW/cm^2 and 10 GW/cm^2.

plasma propagation regime. However, the ionization degree of argon in the plasma induced by low irradiance laser (1.2 GW/cm^2) was relatively low and the ionized population of argon decayed rapidly and disappeared at 400 ns. This is because the argon with relatively high excitation threshold was difficult to be excited at such a low laser irradiance. In addition, the shocked gas layer was so rarefied that it was almost transparent to the laser, so the laser could directly pass through and deposit on the vapor plasma. The ionization of argon was caused by interacting with the hot plasma core. In this case, the plasma propagation model was LSC-wave dominated. In this way, we have successfully produced the LSC- and LSD-wave dominant plasmas by using the low and high laser irradiances, respectively.

3.2. Lifetime of species

First, we discussed the lifetime of exited atoms in the plasma. It can be seen from Figs. 3 and 4 that Ar I, Al I and Mg I species in the LSC-wave dominant plasma exist all the time from 100 ns to 800 ns. The reason is that the atoms in the plasma induced by such low laser irradiation were not completely ionized during the initial expansion of plasma, while in the late stage of plasma cooling, the lifetime of atom was relatively long due to the recombination of ions. For LSD-wave dominant plasma, Mg I and Ar I appeared at 100 ns, while Al I did not appear until 150 ns, because the ionization energy of Al I (5.99 eV) is lower than those of Ar I (15.76 eV) and Mg I (7.65 eV). After the termination of the laser pulse, the Al atoms were completely ionized, and then the atomic Al lines appeared as the expansion and cooling of plasma.

Then the lifetime of exited ions in the plasma was discussed below. It is noticed from Figs. 3 and 4 that for LSD-wave dominant plasma, Mg II and Ar II disappear at 800 ns, while Al II still exists. And all the ions in LSC-wave dominant plasma disappear at 400 ns, which is faster than those in LSD-wave dominant plasma. This is because the higher laser irradiance can improve the degree of ionization, thus reducing the cooling rate of plasma and prolonging the lifetime of ions.

To further analyze the decay process of ionic lines in the plasmas dominated by these two regimes, we integrated the intensities of the emissivity images at corresponding delay. And then, to obtain the integrated intensities on the unit time interval, they were divided by the corresponding gate widths. According to the curve between ICCD gain and signal intensity, the average intensities obtained under different experimental conditions were further corrected. The decays of the emission from Ar, Al and Mg ions in the two regimes of plasmas generated by laser irradiances of 1.2 GW/cm^2 (Fig. 6a) and 10 GW/cm^2 (Fig. 6b) in 100–800 ns are shown in Fig. 6. The time evolutions of the intensity of all ionic lines show the classical exponential decay behavior [25], and the linear correlation coefficients R^2 of these fitting curves are greater than 0.98. It is particularly noted that the smaller the time constant is, the faster the emission lines decay. For example, for the LSC-wave dominant plasma, the Ar II line with time constant of 59 ns decayed faster than Al II and Mg II lines with time constant of 62 ns, while for LSD-wave dominant plasma, the Mg II line with time constant of 107 ns decreased more rapidly than Ar II line with time constant of 134 ns and Al II line with time constant of 190 ns. In addition, the decay of Ar ions in LSC-wave dominant plasma was much faster than that in LSD-wave dominant plasma, which is also evidence of different LSA-wave dominated regimes.

As we know that the intensity I of an emission line can be expressed as

$$I = C' \frac{N}{\lambda_{ij}} \frac{g_i A_{ij}}{U(T)} \exp\left(-\frac{E_i}{k_b T}\right) \quad (1)$$

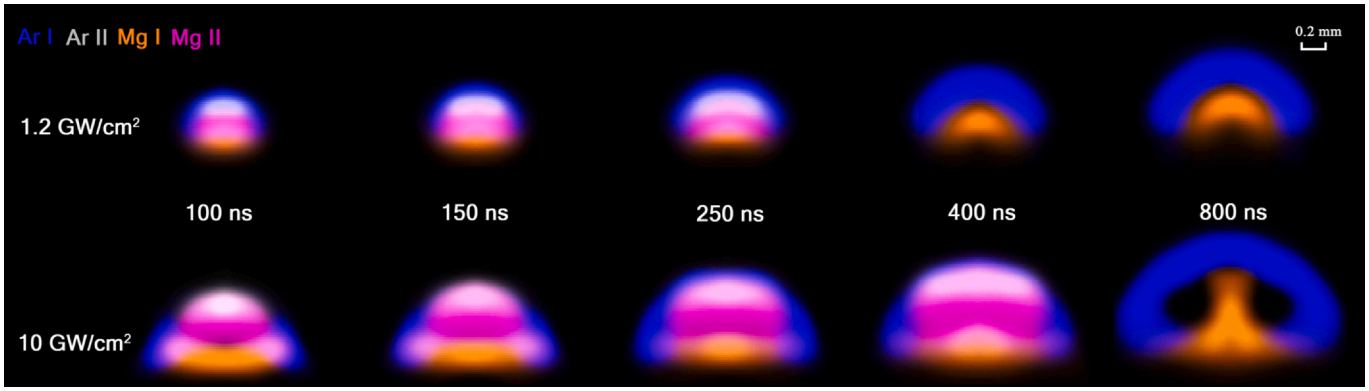

Fig. 4. Emissivity images of Ar I, Ar II, Mg I, and Mg II species in plasmas produced from the Al-Mg alloy at 100, 150, 200, 400, and 800 ns by laser irradiances of 1.2 GW/cm^2 and 10 GW/cm^2.

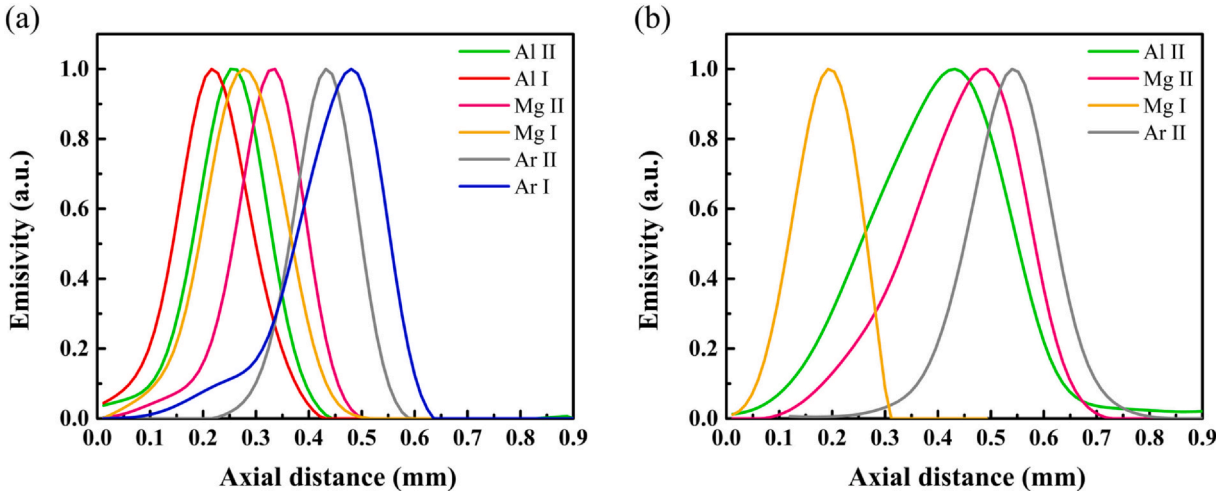

Fig. 5. Normalized central axial emissivity profiles of Ar I, Ar II, Al I, Al II, Mg I, and Mg II species in plasmas produced by laser irradiances of 1.2 GW/cm^2 (Fig. 5a) and 10 GW/ cm^2 (Fig. 5b) at 100 ns.

where C' is a constant, N is the number density, $U(T)$ is the partition function for the emitting species, λ is the wavelength, A is the transition probability, g is the degeneracy, E_i is the upper level energy, k_b is the Boltzmann constant, and T is the plasma temperature. If only spontaneous radiation is considered, the number density N as a function of time t can be expressed as

$$N = N_0 \exp\left(-\sum_j A_{ij} t\right) \tag{2}$$

where N_0 is the initial number density. Then Eq. (1) can be rewritten as

$$I = C' \frac{N_0}{\lambda_{ij}} \frac{g_i A_{ij}}{U(T)} \exp\left(-\frac{E_i}{k_b T}\right) \exp\left(-\sum_j A_{ij} t\right) \tag{3}$$

where the exponential decay can be observed for I, and the transition probability is the key to the decay rate of intensity. However, in the process of radiation, excited atoms (or ions) are constantly produced due to the physical mechanisms such as the recombination of electrons and ions, the collisional excitation of atoms in low-energy and collisional de-excitation of atoms (ions) in high-energy. In other words, the decay of LIBS signal was not only related to the transition probability of lines, but also to the number density of species in the upper energy level. That is why the time constant of ions in LSD-wave dominant plasma was longer than those in LSC-wave dominant plasma.

The transition probabilities of spectral lines are 23.5 × 10^7 s^{-1} for Al II 358.66 nm, 23.2 × 10^7 s^{-1} for Mg II 448.11 nm and 448.13 nm, 8.49 × 10^7 s^{-1} and 8.23 × 10^7 s^{-1} for Ar II 484.78 nm and 487.99 nm, respectively. It can be found that the reduction rate of ions in LSC-wave dominant plasma is associated with the transition probability, and the slow reduction rate of ions is related to the high transition probability. The internal temperature of LSC-wave dominant plasma induced by such low laser irradiance was relatively low and the collision between the species was very weak. Hence, in this case, the main radiation mechanism of LIP was spontaneous radiation. But in LSD-wave dominant plasma, the reduction rate of ions was little dependent on transition probability. The higher internal temperature of plasma induced by intense laser irradiance led to stronger collision between species, and the number density of Mg in LIP was much less than that of Al, assuming that LIP completely carried the sample information and the atomic density ratio of Al to Mg in LIP was also 44:1. On account of the fact that the collision probability of Mg was relatively lower than that of Al, the decay of Mg II was faster than that of Al II. Moreover, the decay of Mg II was also faster than that of Ar II. The most obvious reason for this phenomenon is that the shielding effect of LSD-wave dominant plasma mainly occurred in the shocked gas layer, which led to a strong absorption of the tailing part of laser pulse in argon and the increase of

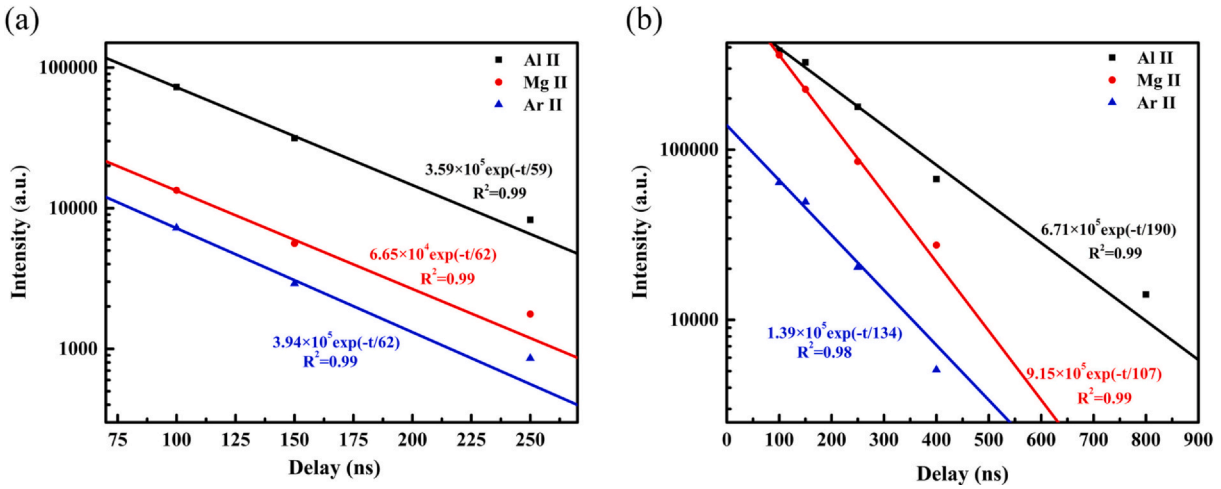

Fig. 6. Decay of the emission intensities of ionic Ar, Al and Mg in plasmas induced by laser irradiances of 1.2 GW/cm^2 (Fig. 6a) and 10 GW/cm^2 (Fig. 6b). The curves are fitted by exponential decay functions.

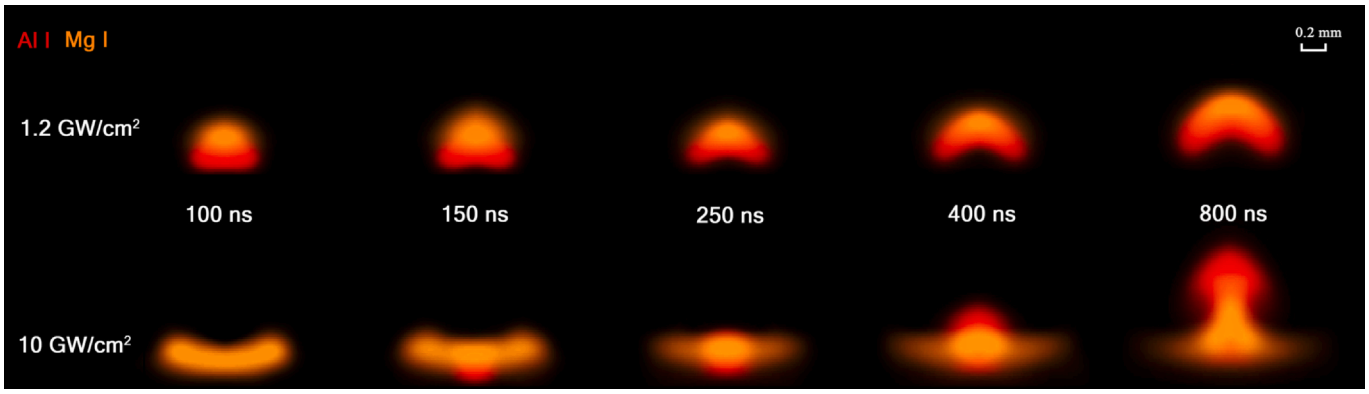

Fig. 7. Emissivity images of Al I and Mg I species in plasmas produced from the Al-Mg alloy at 100, 150, 200, 400, and 800 ns by laser irradiances of 1.2 GW/cm^2 and 10 GW/cm^2.

number density of Ar ions in the upper level.

In summary, to a great extent, the reduction rate of species in LSC-wave dominated plasma is associated with the transition probability, while the most significant factor is the number density of species in the upper energy level for LSD-wave dominated plasma.

3.3. Dependence on LSA-wave regime

To compare the evolution of the vapor plasma composed of four species from the alloy under different ablation conditions, the emissivity images of Al I, Mg I (Fig. 7) and Al II, Mg II (Fig. 8) species in plasmas produced from the Al-Mg alloy at 100, 150, 200, 400, and 800 ns by laser irradiances of 1.2 GW/cm^2 and 10 GW/cm^2 are given. The similar distribution of vapor plasma at initial expansion can be identified for the two regimes. At the low irradiance, the species layers of Al were distributed below those of Mg, while at the high irradiance, the distribution of species layers is similar to that at low irradiance, but the overlap was much more pronounced.

The spectral diagnosis was employed to verify the above inference. The amplified images of the plasmas produced at 250 ns with gate of 100 ns by laser irradiances of 1.2 GW/cm^2 and 10 GW/cm^2 were scanned point by point by the fiber along x axis of plume expansion at $r = 0$ with a 0.5 mm step size. Fig. 9 depicts the normalized intensity of atomic lines of Mg I 518.36 nm and Al I 396.15 nm along x axis. It can be seen that for laser irradiance of 1.2 GW/cm^2, the maximum intensity appeared at x = 0.4 mm for Mg I and at x = 0.3 mm for Al I. This indicates that the Mg species were mainly distributed in the top of LSC-wave dominated plasma. The difference of distribution between the layers of Mg and Al in the plasma produced by laser irradiance of 10 GW/cm^2 was not obvious, and the maximum intensity for them was at the axial position of 0.4 mm. This may be due to the expansion of the plasma, which made the difference less significant at 250 ns. The results are consistent with the image of Mg I and Al I at 250 ns as shown in Fig. 7.

In our previous work [23], for immiscible alloys, the species with a lower melting point are preferentially separated from the sample during laser ablation and distributed at an upper shell of the plasma. The melting points of constituted elements heavily influence the species distribution in LSC-wave dominated plasma induced by immiscible alloy, while atomic mass is a crucial factor that determines the relative species distribution in LSD-wave dominated plasma. However, the physical property of the miscible alloy used in this experiment is different from that of the immiscible alloy, and it has no liquid phase separation characteristics. The above features of distribution are in agreement with the physical intuition of the two elements (listed in Table 1). For LSC-wave dominated plasma, the Al and Mg will be melted simultaneously once the temperature of laser ablation zone reaches the melting point of the alloy. But Mg (1363 K) has a much lower boiling point than Al (2740 K), thus the Mg species are firstly vaporized and distributed in the upper part of the vapor plasma. For LSD-wave dominated plasma, the excessive laser irradiation directly vaporizes all the species on the alloy surface. In this way, the velocities of species are the most significant factor in the species distribution in plasma. The relative atomic mass of Mg (24) is slightly lower than that of Al (27), thus the layers of Mg species is slightly higher than those of Al species with a serious overlap. In this case, the species distribution in LSC-wave dominated plasma induced by miscible alloy is related to the boiling point, while in LSD-wave dominated plasma it is related to the atomic mass.

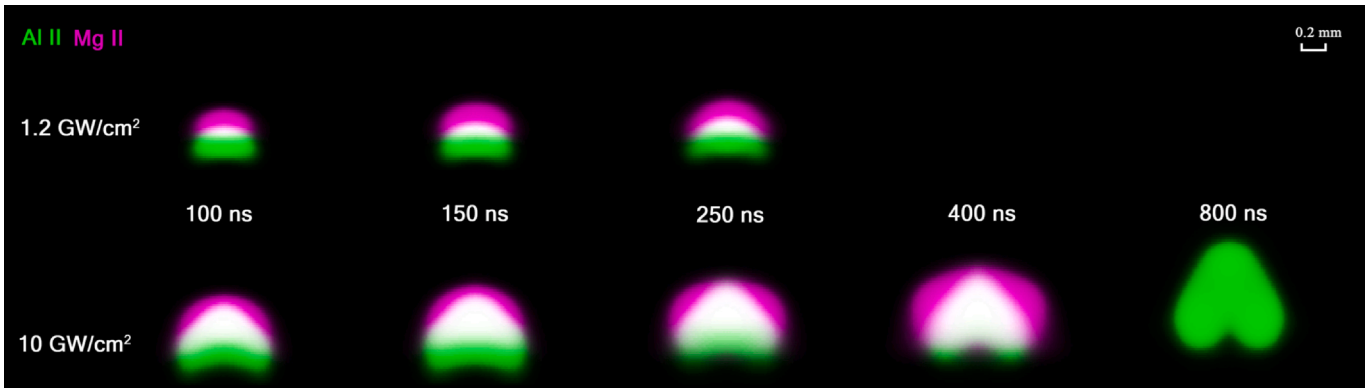

Fig. 8. Emissivity images of Al II and Mg II species in plasmas produced from the Al-Mg alloy at 100, 150, 200, 400, and 800 ns by laser irradiances of 1.2 GW/cm^2 and 10 GW/cm^2.

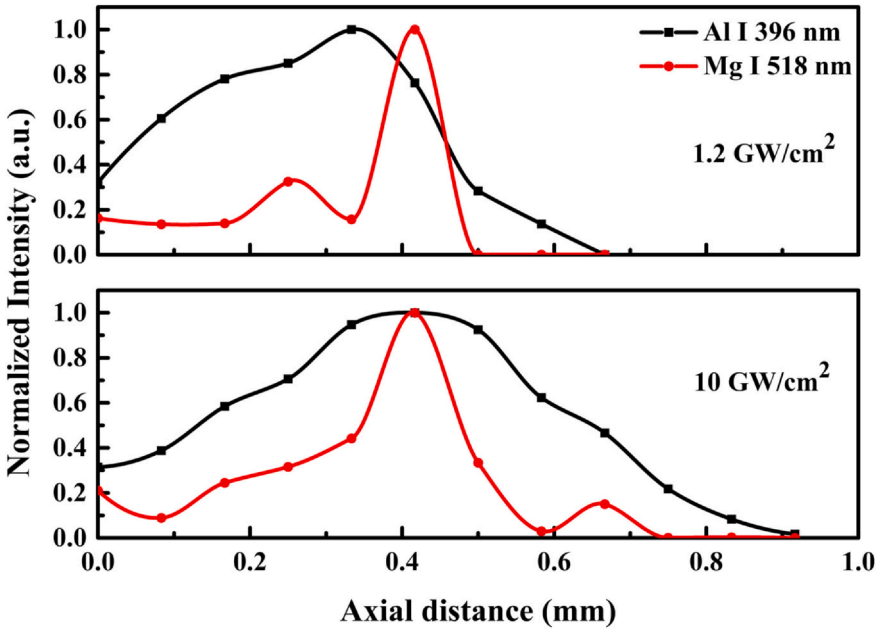

Fig. 9. Normalized intensity of Mg I and Al I along x axis of the plasma produced by laser irradiances of 1.2 GW/cm^2 and 10 GW/cm^2 at 250 ns.

4. Conclusion

In this paper, the structure and dynamics of laser-induced plasmas on binary miscible alloys immersed in argon ambient of atmospheric pressure were investigated by spectrally, spatially and temporally resolved imaging. The dependence of species distribution in plasma produced from miscible alloy on LSA-wave regime and the lifetimes of species in different ablation conditions were studied. At relatively low laser irradiance, in which case the plasma propagation is characterized by LSC-wave regime, the reduction rate of species is to a great extent associated with the transition probability. Boiling point is the key factor that determines the relative species distribution in the initial plasma. For miscible alloys, all the species are melted simultaneously, and the species with lower boiling point are preferentially vaporized and distributed in the upper part of the vapor plasma. At high laser irradiance, when the plasma propagation exhibits characteristics corresponding to LSD-wave, the number density of species in the upper energy level is the major factor affecting the reduction rate of species. Atomic mass is a crucial factor that determines the relative species distribution in plasma. Species with smaller atomic mass have the faster movement velocity and are distributed at an upper shell of the plasma. In summary, we have revealed the effect of species distribution in plasma generated by binary miscible and immiscible alloys on the LSA-wave regime, and the dependence of species distribution in plasmas produced from more complex materials deserves further study.

Declaration of Competing Interest

The authors declare that they have no known competing financial interests or personal relationships that could have appeared to influence the work reported in this paper.

Acknowledgments

National Key R&D Program of China (2017YFA0304203); National Energy R&D Center of Petroleum Refining Technology (RIPP, SINOPEC); Changjiang Scholars and Innovative Research Team in University of Ministry of Education of China (IRT_17R70); National Natural Science Foundation of China (NSFC) (61975103, 61875108, 61775125, 11434007); Major Special Science and Technology Projects in Shanxi (201804D131036); 111 project (D18001); Fund for Shanxi "1331KSC"; Achievements transformation project of universities in Shanxi Province (2020CG003). The name of the institute or organization that provided the funding is Shanxi provincial education department. The beneficiary is Suotang Jia.

References

[1] D.H. Lowndes, D.B. Geohegan, A.A. Puretzky, D.P. Norton, C.M. Rouleau, Synthesis of novel thin-film materials by pulsed laser deposition, Science 273 (5277) (1996) 898–903.
[2] H.U. Krebs, M. Weisheit, J. Faupel, E. Süske, M. Buback, Pulsed Laser Deposition (PLD)-a Versatile Thin Film Technique, Advances in Solid State Physics, Springer, 2003, pp. 510–518.
[3] Z.Y. Hou, Z. Wang, T.B. Yuan, J.M. Liu, Z. Li, W.D. Ni, A hybrid quantification model and its application for coal analysis using laser induced breakdown spectroscopy, J. Anal. At. Spectrom. 31 (3) (2016) 722.
[4] M. Gaft, E. Dvir, H. Modiano, U. Schone, Laser induced breakdown spectroscopy machine for online ash analysis in coal, Spectrochim. Acta B 63 (10) (2008) 1177–1182.
[5] Z. Lei, Y. Gong, Y.F. Li, X. Wang, J.J. Fan, L. Dong, W.G. Ma, W.B. Yin, S.T. Jia, Development of a coal quality analyzer for application to power plants based on laser-induced breakdown spectroscopy, Spectrochim. Acta B 113 (2015) 167–173.
[6] A.D. Giacomo, M. Dell'Aglio, D. Bruno, R. Gaudiuso, O.D. Pascale, Experimental and theoretical comparison of single-pulse and double-pulse laser induced breakdown spectroscopy on metallic samples, Spectrochim. Acta B 63 (7) (2008) 805–816.
[7] R.G. Root, Modeling of Post Breakdown Phenomena, Laser-Induced Plasmas and Applications, Dekker, New York, 1989.
[8] X.S. Bai, F. Cao, V. Motto-Ros, Q.L. Ma, Y.P. Chen, J. Yu, Morphology and characteristics of laser-induced aluminum plasma in argon and in air: a comparative study, Spectrochim. Acta B 113 (2015) 158–166.
[9] Q.L. Ma, V. Motto-Ros, X.S. Bai, J. Yu, Experimental investigation of the structure and the dynamics of nanosecond laser-induced plasma in 1-atm argon ambient gas, Appl. Phys. Lett. 103 (20) (2013) 1–5.
[10] X.S. Bai, Q.L. Ma, M. Perrier, V. Motto-Ros, Y. Jin, Experimental study of laser-induced plasma: influence of laser fluence and pulse duration, Spectrochim. Acta B 87 (9) (2013) 27–35.
[11] J. Yu, Q.L. Ma, V. Motto-Ros, W.Q. Lei, X.C. Wang, X.S. Bai, Generation and expansion of laser-induced plasma as a spectroscopic emission source, Front. Phys. 7 (6) (2012) 649–669.
[12] G.C. Tyrrell, T. York, N. Cherief, D. Givord, I.W. Boyd, Kinetic energy and mass distribution of ablated species formed during pulsed laser deposition, Microelectron. Eng. 25 (2–4) (1994) 247–252.
[13] G. Cristoforetti, G. Lorenzetti, S. Legnaioli, V. Palleschi, Investigation on the role of air in the dynamical evolution and thermodynamic state of a laser-induced aluminium plasma by spatial- and time-resolved spectroscopy, Spectrochim. Acta B 65 (9–10) (2010) 787–796.
[14] S.S. Harilal, G.V. Miloshevsky, P.K. Diwakar, N.L. Lahaye, A. Hassanein, Experimental and computational study of complex shockwave dynamics in laser ablation plumes in argon atmosphere, Phys. Plasmas 19 (8) (2012) 083504.

[15] S.S. Harilal, C.V. Bindhu, M.S. Tillack, F. Najmabadi, A.C. Gaeris, Internal structure and expansion dynamics of laser ablation plumes into ambient gases, J. Appl. Phys. 93 (5) (2003) 2380–2388.
[16] J.A. Aguilera, C. Aragón, Characterization of laser-induced plasma during its expansion in air by optical emission spectroscopy: observation of strong explosion self-similar behavior, Spectrochim. Acta B 97 (2014) 86–93.
[17] J.A. Aguilera, C. Aragón, Characterization of a laser-induced plasma by spatially resolved spectroscopy of neutral atom and ion emissions. Comparison of local and spatially integrated measurements, Spectrochim. Acta B 59 (12) (2004) 1861–1876.
[18] V. Bulatov, L. Xu, I. Schechter, Spectroscopic imaging of laser-induced plasma, Anal. Chem. 68 (17) (1996) 2966–2973.
[19] R.A. Al-Wazzan, J.M. Hendron, T. Morrow, Spatially and temporally resolved emission intensities and number densities in low temperature laser-induced plasmas in vacuum and in ambient gases, Appl. Surf. Sci. 96 (95) (1996) 170–174.
[20] D.A. Cremers, L.E. Foster, M.J. Ferris, R.A. Multari, Effect of sampling geometry on elemental emissions in laser-induced breakdown spectroscopy, Appl. Spectrosc. 50 (12) (1996) 1483–1499.
[21] V. Motto-Ros, Q.L. Ma, S. Grégoire, W.Q. Lei, X.C. Wang, F. Pelascini, F. Surma, V. Detalle, J. Yu, Dual-wavelength differential spectroscopic imaging for diagnostics of laser-induced plasma, Spectrochim. Acta B 74-75 (2012) 11–17.
[22] Q.L. Ma, V. Motto-Ros, W.Q. Lei, M. Boueri, X.S. Bai, L.J. Zheng, H.P. Zeng, J. Yu, Temporal and spatial dynamics of laser-induced aluminum plasma in argon background at atmospheric pressure: interplay with the ambient gas, Spectrochim. Acta B 65 (11) (2010) 896–907.
[23] Y. Zhao, L. Zhang, J.J. Hou, W.G. Ma, L. Dong, W.B. Yin, L.T. Xiao, S.T. Jia, J. Yu, Species distribution in laser-induced plasma on the surface of binary immiscible alloy, Spectrochim. Acta B 158 (2019) 105644.
[24] S.L. Ma, H.M. Gao, L. Wu, Modified fourier-hankel method based on analysis of errors in abel inversion using fourier transform techniques, Appl. Opt. 47 (9) (2008) 1350–1357.
[25] V.I. Babushok, F.C. Delucia, P.J. Dagdigian, M.J. Nusca, A.W. Miziolek, Kinetic Modeling of the laser-induced breakdown spectroscopy plume from metallic lead, Appl. Opt. 42 (30) (2003) 5947–5962.